METHODOLOGY OF TIME-LAPSE ELASTIC FULL-WAVEFORM INVERSION FOR VTI MEDIA

YANHUA LIU and ILYA TSVANKIN

Center for Wave Phenomena, Colorado School of Mines, Golden, CO 80401, U.S.A.
liuyanhua@mymail.mines.edu; ilya@mines.edu.

(Received July 15, 2020; revised version accepted January 10, 2021)

ABSTRACT

Liu, Y.H. and Tsvankin, I., 2021. Methodology of time-lapse elastic full-waveform inversion for VTI media. *Journal of Seismic Explorarion*, 30: 257-270.

Time-lapse seismic processing can provide important information about the variations of reservoir properties during hydrocarbon production and CO_2 injection. High-resolution results for time-lapse seismic can potentially be obtained from full-waveform inversion (FWI), but most existing time-lapse FWI methods are limited to isotropic and, often, acoustic media. Extension of these techniques to more realistic anisotropic elastic models is hampered by the trade-offs between the medium parameters and significantly increased computational cost. Here, we develop a time-lapse FWI algorithm for VTI (transversely isotropic with a vertical symmetry axis) media and evaluate several strategies of applying it to multicomponent and pressure data. The adjoint-state method and a nonlinear conjugate-gradient technique are employed to derive the gradient of the objective function and update the model parameters. We test the algorithm on a relatively simple VTI graben model using the parallel-difference, sequential-difference and double-difference time-lapse methods. The results confirm the ability of the proposed technique to reconstruct localized time-lapse parameter variations in anisotropic media with sufficient spatial resolution. The double-difference approach proves to be more accurate than the other methods in reconstructing the time-lapse variations from noise-free multicomponent data. When FWI operates with clean pressure data, the parallel-difference method is generally more accurate than the other techniques, especially in estimating the shear-wave vertical velocity V_{S0}. For multicomponent and pressure data contaminated with realistic noise, the double-difference method produces large errors in the temporal variations of the VTI parameters. The parallel-difference technique outperforms its sequential-difference counterpart in reconstructing the time-lapse variations inside the target zone from the noisy data while the latter approach performs better in suppressing the false artifacts outside the "reservoir". The tests also demonstrate that including more information in time-lapse FWI does not always improve the inversion results, likely due to the increased multimodality of the objective function.

KEY WORDS: time-lapse seismic, full-waveform inversion (FWI), multicomponent data, elastic inversion, anisotropy, VTI media.

0963-0651/21/$5.00

INTRODUCTION

Time-lapse (4D) seismic has become a common tool for optimizing hydrocarbon reservoir production and CO_2 injection (Lumley et al., 2010; Smith and Tsvankin, 2013, 2016; Pevzner et al., 2017). Processing of time-lapse data can provide important information about the variations of the reservoir properties, such as pressure and fluid saturation.

Full-waveform inversion has been successfully applied to velocity analysis and reservoir characterization (Vigh et al., 2014; Asnaashari et al., 2015; Singh et al., 2018) and can potentially provide estimates of time-lapse parameter variations with high spatial resolution. Among the proposed strategies of time-lapse FWI are the parallel-difference (Plessix et al., 2010), sequential-difference, and double-difference methods (Watanabe et al., 2004; Denli and Huang, 2009), as well as joint (Alemie and Sacchi, 2016) and simultaneous (Maharramov and Biondi, 2014) inversion techniques. The parallel-difference method uses the same initial model for the baseline and monitor inversions, while the sequential-difference method employs the inverted baseline data to build the initial model for the inversion of the monitor data. The double-difference technique directly estimates the time-lapse data difference starting with the inverted baseline model.

However, most published time-lapse FWI algorithms are limited to isotropic and, sometimes, acoustic media. Extension of these methods to more realistic anisotropic models involves serious challenges, including the much higher computational cost and the trade-offs between multiple parameters needed to describe anisotropic formations (Kamath and Tsvankin, 2016; Singh et al., 2018).

Here, we present a time-lapse FWI methodology for VTI media and test it on a relatively simple graben model, where the "reservoir" is located in thin dipping layers. Three most common time-lapse approaches are applied to estimate the temporal variations of the VTI parameters using both multicomponent and pressure data. Analysis of the inversion results reveals the advantages and shortcomings of the employed strategies in reconstructing the time-lapse VTI model.

METGODOLOGY OF TIME-LAPSE FWI FOR VTI MEDIA

The goal of time-lapse FWI is to estimate the temporal variations of the medium parameters using seismic data before (baseline survey) and during or after (monitor survey) hydrocarbon production or CO_2 injection. We parameterize VTI media by the velocities V_{P0} (P-wave vertical velocity), V_{S0} (S-wave vertical velocity), $V_{hor,P}$ (P-wave horizontal velocity), $V_{nmo,P}$ (P-wave normal-moveout velocity from a horizontal reflector), and density ρ.

These parameters fully describe the properties of P- and SV-waves for vertical transverse isotropy. The advantages of this notation for elastic FWI of multicomponent reflection data are discussed by Kamath et al. (2017). The velocities $V_{hor,P}$ and $V_{nmo,P}$ are expressed through the Thomsen parameters ε and δ as follows (Thomsen, 1986; Tsvankin, 2012):

$$V_{\mathrm{hor,P}} = V_{\mathrm{P0}}\sqrt{1+2\varepsilon}\ , \tag{1}$$

$$\mathrm{V_{nmo,P}} = \mathrm{V_{P0}}\sqrt{1+2\delta}\ . \tag{2}$$

Typically, a conventional FWI algorithm is applied to the baseline data, while the monitor survey can be processed using several different approaches mentioned above. Here, we focus on the parallel-, sequential-, and double-difference methods, which share the same L_2-norm objective function (e.g., Tarantola, 1984) for the inversion of the baseline (subscript b) data:

$$\mathrm{S_b}(\mathbf{m}) = \frac{1}{2}\left\|\mathbf{W}_\mathrm{b}\left[\mathbf{d}_\mathrm{b}^{\mathrm{sim}}(\mathbf{m}_\mathrm{b}) - \mathbf{d}_\mathrm{b}^{\mathrm{obs}}\right]\right\|^2\ , \tag{3}$$

where $\mathbf{d}_\mathrm{b}^{\mathrm{sim}}$ is the data simulated for the baseline model $\mathbf{m}_\mathrm{b}$, $\mathbf{d}_\mathrm{b}^{\mathrm{obs}}$ is the observed data, and $\mathbf{W}_\mathrm{b}$ is the weighting data-misfit operator.

To simulate multicomponent seismic data, we solve the 2D elastic wave equation for arbitrarily heterogeneous VTI media with a fourth-order finite-difference algorithm. Model updating based on the objective function in eq. (3) is performed with the conjugate-gradient technique, and FWI is implemented using a multiscale approach (Bunks et al., 1995).

The three strategies examined here differ in the way they handle the monitor survey or the time-lapse data difference, as described in more detail below.

Parallel-difference method

In the parallel-difference approach (Plessix et al., 2010), the baseline and monitor inversions are performed independently but with the same initial model. Then the time-lapse variation in each parameter is obtained by subtracting the inversion results for the two surveys. If the errors in the inverted baseline and monitor models are similar (for example, have the same sign), they will be reduced (partially canceled) by the subtraction. In that case, the time-lapse model produced by the parallel-difference method may remain sufficiently accurate.

Sequential-difference method

The sequential-difference strategy (Asnaashari et al., 2012) uses the inverted baseline model as the initial model in FWI of the monitor data. Because the time-lapse variation is largely confined to the reservoir, the baseline model should provide a good approximation for the parameters obtained from the monitor data outside the target area. Then, as in the parallel-difference method, the inverted baseline parameters are subtracted from those for the monitor survey.

By starting the reconstruction of the time-lapse parameters with the inverted baseline model, the sequential-difference method speeds up the convergence of the updating algorithm and partially mitigates parameter trade-offs and problems caused by local minima of the objective function. However, this approach relies on an accurate estimation of the baseline model, which might be problematic, for example, if the baseline data are noisy.

Double-difference method

In the double-difference method (Watanabe et al., 2004; Denli and Huang, 2009), FWI is first applied to the baseline data $\mathbf{d}_{\mathrm{b}}^{\mathrm{obs}}$ to obtain the inverted baseline model $\mathbf{m}_{\mathrm{b}}^{\mathrm{inv}}$. Next, the so-called "composite" data set $\mathbf{d}_{\mathrm{com}}$ is generated by adding the observed time-lapse variations $\mathbf{d}_{\mathrm{m}}^{\mathrm{obs}} - \mathbf{d}_{\mathrm{b}}^{\mathrm{obs}}$ to the wavefield simulated for the inverted baseline model. Then FWI operates directly with the time-lapse response by minimizing the difference $\Delta\mathbf{d}$ between the "composite" data $\mathbf{d}_{\mathrm{com}}$ and the simulated monitor data $\mathbf{d}_{\mathrm{m}}^{\mathrm{sim}}$, starting from the inverted baseline model:

$$\Delta\mathbf{d} = \left(\mathbf{d}_{\mathrm{m}}^{\mathrm{obs}} - \mathbf{d}_{\mathrm{b}}^{\mathrm{obs}}\right) - \left(\mathbf{d}_{\mathrm{m}}^{\mathrm{sim}} - \mathbf{d}_{\mathrm{b}}^{\mathrm{sim}}\right) = \mathbf{d}_{\mathrm{com}} - \mathbf{d}_{\mathrm{m}}^{\mathrm{sim}} , \qquad (4)$$

$$\mathbf{d}_{\mathrm{com}} = \mathbf{d}_{\mathrm{m}}^{\mathrm{obs}} - \mathbf{d}_{\mathrm{b}}^{\mathrm{obs}} + \mathbf{d}_{\mathrm{m}}^{\mathrm{sim}} . \qquad (5)$$

Finally, the time-lapse parameter variations are obtained by subtracting the inverted baseline model from the reconstructed "composite" (i.e., monitor) model.

SYNTHETIC EXAMPLES

The proposed time-lapse FWI algorithm is tested on a 2D VTI model that includes a graben structure (Figs. 1a, 1d, 1g, 1j, 1m). The time-lapse parameters for the monitor survey are obtained by reducing the baseline velocities V_{P0} and V_{S0} in the target area (i.e., in the dipping layer segments) by approximately 13%, and density ρ by 10% (Figs. 1c, 1f, 1i, 1*l*, 1o). The initial baseline parameters are computed by Gaussian smoothing of the actual parameter distributions (Figs. 1b, 1e, 1h, 1k, 1n).

The elastic wavefield is excited by 116 shots (which represent point explosions) placed with a constant increment along a horizontal line at a depth of 40 m. The source signal is a Ricker wavelet with a central frequency of 10 Hz. We employ 400 receivers evenly distributed along the horizontal line at a depth of 100 m (Fig. 1a).

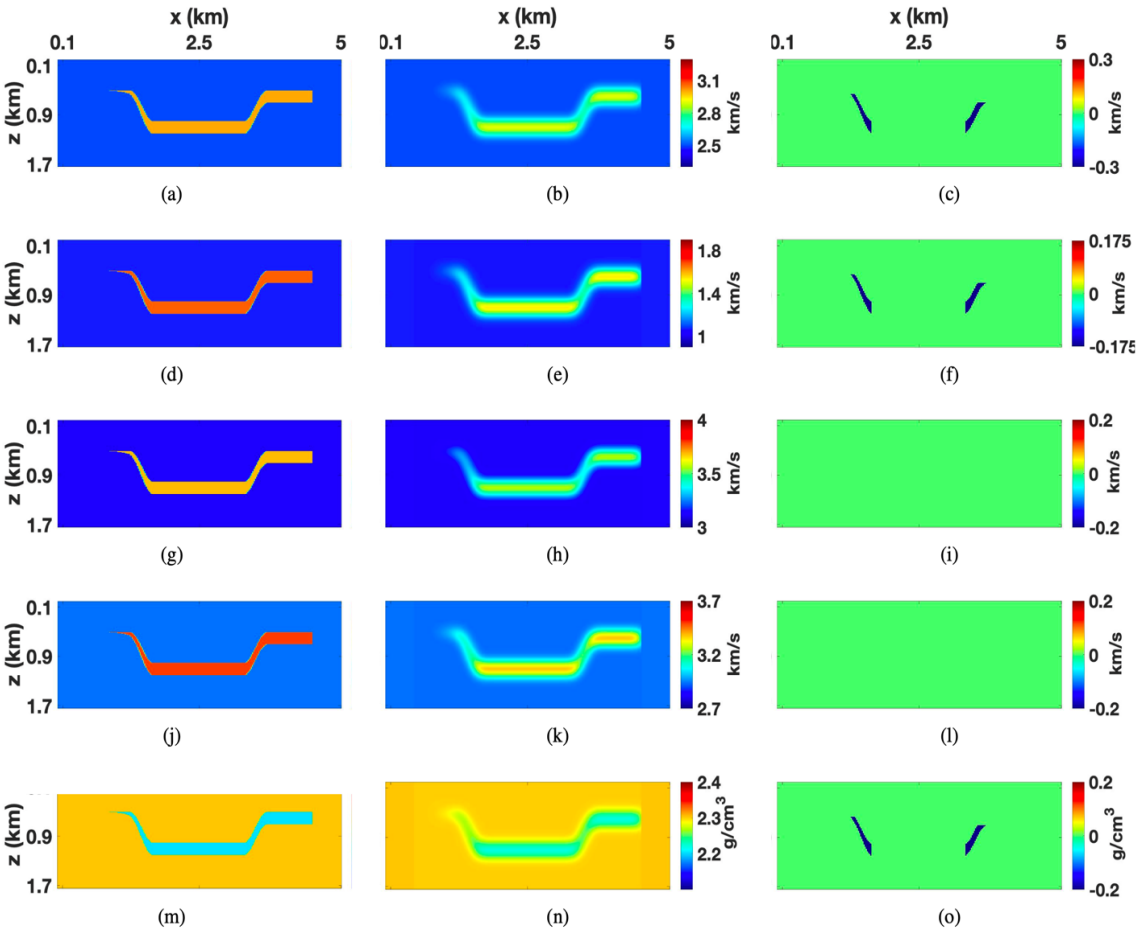

Fig. 1. Parameters of the baseline model with a grid size of 10×10 m: (a) the P-wave vertical velocity (V_{P0}), (d) the S-wave vertical velocity (V_{S0}), (g) the P-wave horizontal velocity ($V_{hor,P}$), (j) the P-wave normal-moveout velocity ($V_{nmo,P}$), and (m) the density (ρ). The initial baseline model of: (b) V_{P0}, (e) V_{S0}, (h) $V_{hor,P}$, (k) $V_{nmo,P}$, and (n) ρ. The actual time-lapse differences for (c) V_{P0}, (f) V_{S0}, (i) $V_{hor,P}$, (l) $V_{nmo,P}$, and (o) ρ.

Following Singh et al. (2019), FWI is performed using a multiscale approach with four frequency bands (2-5 Hz, 2-8 Hz, 2-13 Hz, 2-19 Hz). The low-frequency data (0-2 Hz), which usually are difficult to record in the field, are not included in the inversion. The accuracy of the three time-lapse methods is evaluated by computing the normalized errors in the temporal parameter variations at each grid point.

Multicomponent data

First, the noise-free multicomponent data for the baseline model are inverted using the anisotropic FWI algorithm described above. While the overall accuracy of parameter estimation is satisfactory, there are noticeable errors at and near the boundaries of the graben structure due to edge effects (Fig. 2).

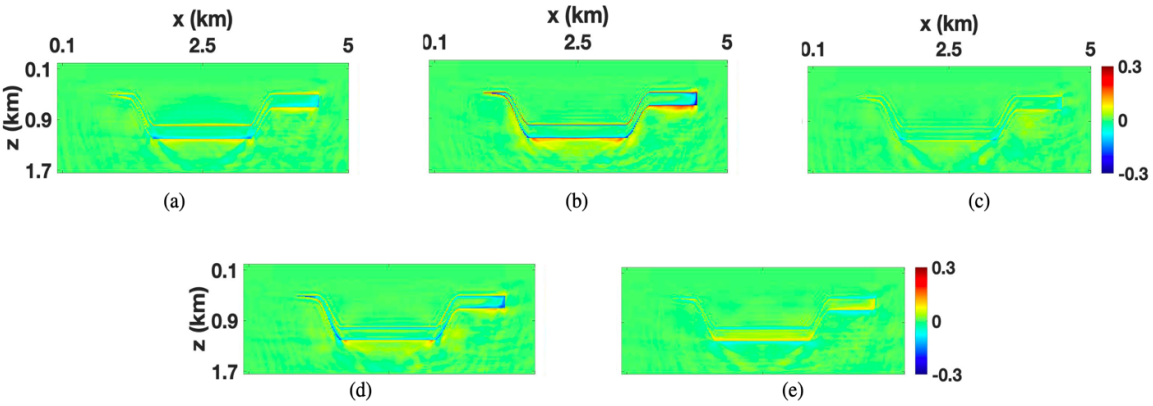

Fig. 2. Normalized parameter errors for the final baseline model reconstructed from the multicomponent data: (a) V_{P0}, (b) V_{S0}, (c) $V_{hor,P}$, (d) $V_{nmo,P}$ and (e) ρ.

Then we apply the parallel-, sequential- and double-difference methods to evaluate the time-lapse variations in the parameters V_{P0}, V_{S0}, and ρ (the NMO and horizontal velocities are held constant). In our application of the sequential-difference method below, the inverted baseline model for the 2-5 Hz frequency range is used as the initial model for the monitor inversion. Similar to the baseline inversion, all three techniques (Fig. 3) produce errors in the time-lapse variations of V_{P0}, V_{S0}, and ρ near the boundaries of the target area. These errors are caused primarily by the jumps in V_{P0}, V_{S0}, and ρ across the boundaries of the target for the monitor survey and for the "composite" data used in the double-difference method.

Outside the target area, the double-difference method (Figs. 3c, 3f, 3o) yields more accurate estimates of V_{P0}, V_{S0}, and ρ (i.e., it shows no changes) than the other methods (Figs. 3a, 3d, 3m, 3b, 3e, 3n) because it is specifically designed for inverting the time-lapse data variations. The three methods reconstruct the time-lapse changes of V_{P0}, V_{S0}, and ρ inside the target zone with similar accuracy.

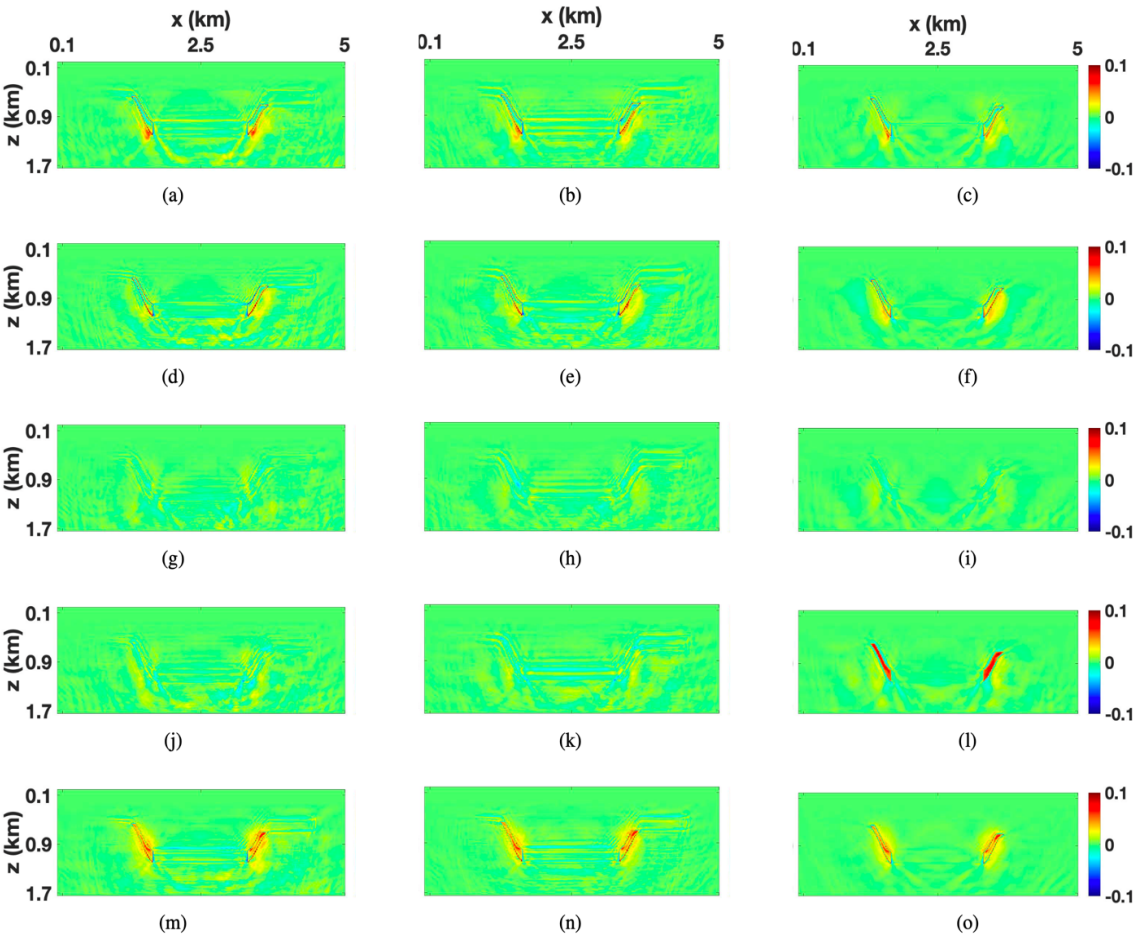

Fig. 3. Normalized errors of the time-lapse parameter variations obtained from the noise-free multicomponent data using three different approaches. Only the parameters V_{P0}, V_{S0}, and ρ are changed. The parallel-difference method: (a) V_{P0}, (d) V_{S0}, (g) $V_{hor,P}$, (j) $V_{nmo,P}$, and (m) ρ. The sequential-difference method: (b) V_{P0}, (e) V_{S0}, (h) $V_{hor,P}$, (k) $V_{nmo,P}$, and (n) ρ. The double-difference method: (c) V_{P0}, (f) V_{S0}, (i) $V_{hor,P}$, (l) $V_{nmo,P}$, and (o) ρ.

Although there are no temporal variations in the velocities $V_{hor,P}$ and $V_{nmo,P}$, all methods generate false time-lapse anomalies in them (Figs. 3g, 3j, 3h, 3k, 3i, 3*l*) because of the parameter trade-offs. As is the case for the inversion results for V_{P0}, V_{S0}, and ρ, the false anomalies in $V_{hor,P}$ and $V_{nmo,P}$ (Figs. 3i, 3*l*) are less pronounced (and mainly located near the target

boundaries) in the output of the double-difference method. In contrast, the errors in $V_{hor,P}$ and $V_{nmo,P}$ produced by the parallel- and sequential-difference approaches are observed not only near the target boundaries, but also beneath the graben structure. The double-difference method, however, generates a pronounced false perturbation in $V_{nmo,P}$ inside the target zone (Fig. 3*l*).

To analyze the leakage (i.e., the trade-offs) between the temporal variations of different parameters, next we change only one parameter (V_{P0}, V_{S0}, or ρ) at a time. Here, we discuss just the test for the perturbation in the velocity V_{S0}; the results for the parameters V_{P0} and ρ are generally similar. Interestingly, the time-lapse inversion errors in this test (Fig. 4) are larger compared to the previous experiment in which we changed three parameters. Apparently, for this model the distortions related to the temporal variations in several parameters partially compensate one another.

As in the previous test (Fig. 3), the double-difference method produces the most accurate results outside the target area for all parameters (where they remain unchanged), as well as for $V_{hor,P}$ inside the "reservoir" (Fig. 4). Still, there is a significant false anomaly in the velocity $V_{nmo,P}$ (Fig. 4i) in the output of the double-difference algorithm. A similar anomaly in the velocity $V_{nmo,P}$ in the previous test (Fig. 3*l*) is apparently caused by the temporal variation in V_{S0} because it does not appear when we change just the velocity V_{P0} or density ρ.

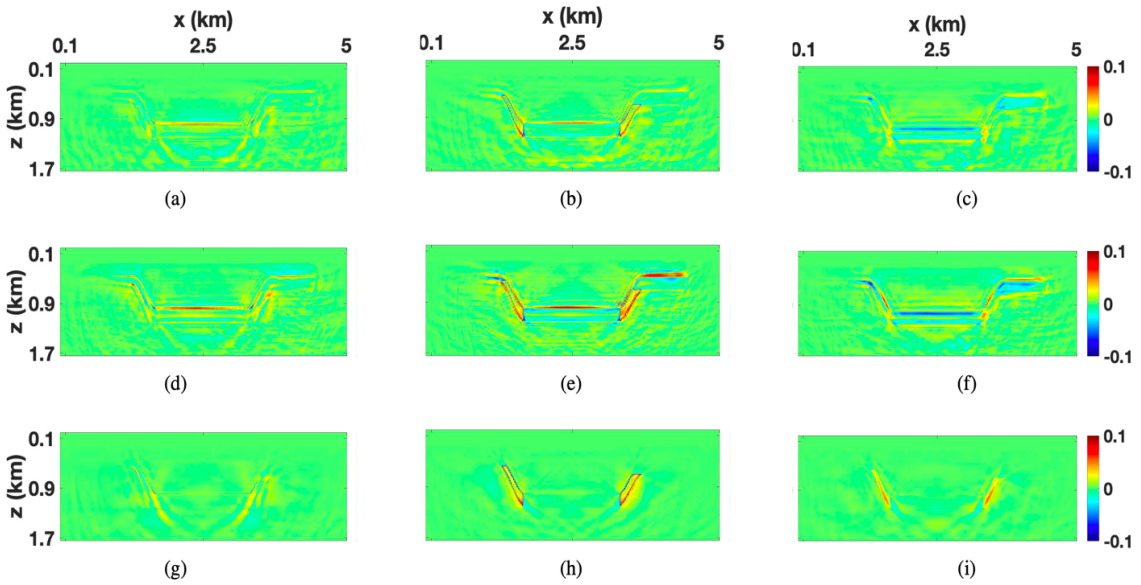

Fig. 4. Normalized errors of the time-lapse parameter variations obtained from the noise-free multicomponent data. Only the parameter V_{S0} is changed. The parallel-difference method: (a) V_{P0}, (b) V_{S0}, and (c) $V_{nmo,P}$. The sequential-difference method: (d) V_{P0}, (e) V_{S0}, and (f) $V_{nmo,P}$. The double-difference method: (g) V_{P0}, (h) V_{S0}, and (i) $V_{nmo,P}$.

Pressure data

Because pressure recordings contain less information than the displacement field (in particular, about shear waves), the resolution of the inverted parameters (Fig. 5) is lower compared to that for the multicomponent data. However, the absence of the false time-lapse anomaly in $V_{nmo,P}$ (Fig. 5*l*) in the results of the double-difference method indicates that FWI of pressure data may be less influenced by the parameter trade-offs. Although adding multicomponent data typically increases parameter resolution, it can also make the objective function more complex and multimodal, which hinders convergence toward the global minimum of the objective function. This observation is also made by Kamath and Tsvankin (2013) who performed elastic FWI for horizontally layered VTI media.

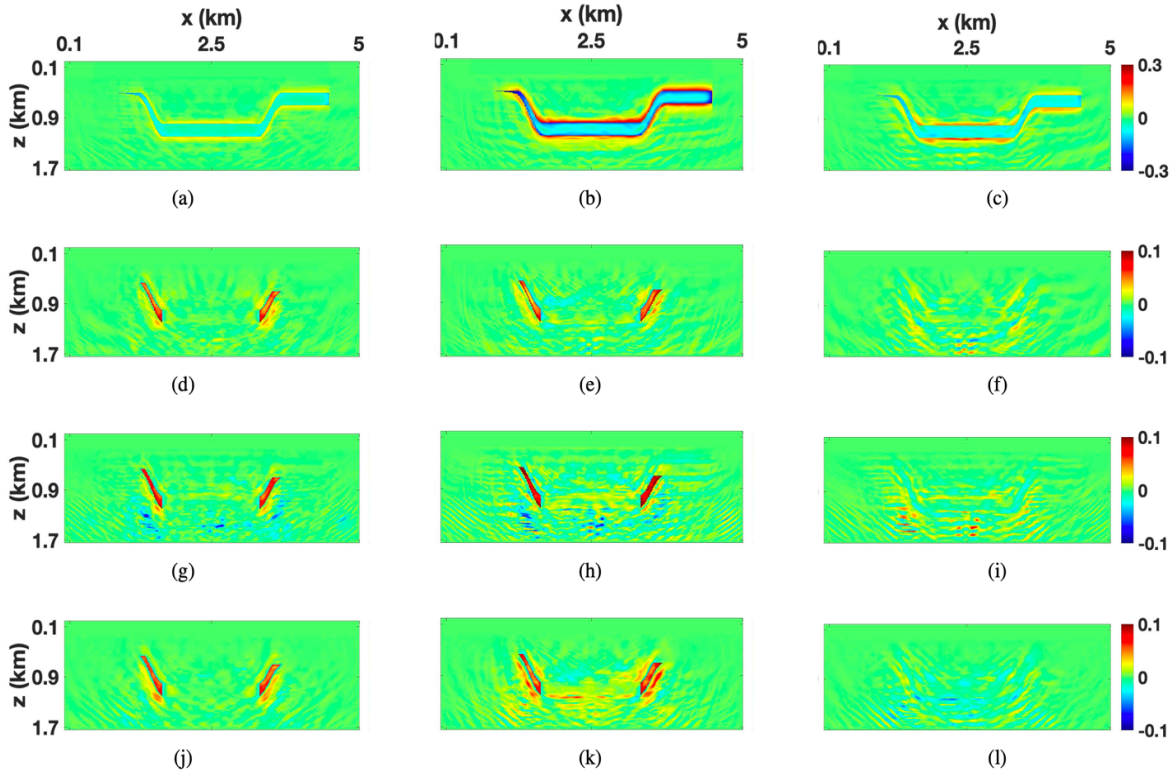

Fig. 5. Baseline models reconstructed from the noise-free pressure data: (a) V_{P0}, (b) V_{S0}, and (c) $V_{nmo,P}$. Normalized errors of the time-lapse parameter variations reconstructed from the noise-free pressure data. Only the parameters V_{P0}, V_{S0}, and ρ are changed. The parallel-difference method: (d) V_{P0}, (e) V_{S0}, and (f) $V_{nmo,P}$. The sequential-difference method: (g) V_{P0}, (h) V_{S0}, and (i) $V_{nmo,P}$. The double-difference method: (j) V_{P0}, (k) V_{S0}, and (*l*) $V_{nmo,P}$.

Note that the algorithm was able to reconstruct the graben structure in the fields of all medium parameters (including density, which is not shown in Fig. 5) because FWI operates with the entire elastic wavefield and the acquisition geometry in our experiment covers a wide range of offsets.

However, the spatial resolution at and below the graben boundaries is noticeably lower than that obtained from the multicomponent data. As a result, the time-lapse variations estimated by the sequential-difference method (Figs. 5g, 5h, 5i) have a lower resolution compared to the other two methods. This is explained by the strong reliance of the sequential-difference approach on the accuracy of the inverted baseline model.

Predictably, for the baseline, monitor, and "composite" data, the results of the pressure inversion are less accurate than those for multicomponent data. However, the errors in the recovered baseline and monitor models are similar and, therefore, partially cancel each other in the output of the parallel-difference method. As a result, the parallel-difference method (Figs. 5d, 5e) outperforms its double-difference counterpart (Figs. 5j, 5k) in suppressing false anomalies in V_{P0}, V_{S0}, and ρ. The advantages of the parallel-difference method are especially obvious in the time-lapse model of V_{S0} because this parameter is not well constrained by FWI of the pressure data (Fig. 5b). The artifacts in the time-lapse variations of the velocities $V_{hor,P}$ and $V_{nmo,P}$ (which are unchanged) for the parallel- and double-difference methods have close magnitudes, but different spatial distributions (Figs. 5f, 5*l*). On the whole, the accuracy of these two methods for the parameters $V_{hor,P}$ and $V_{nmo,P}$ is comparable, but the parallel-difference method yields better estimates of the changes in V_{P0}, V_{S0}, and ρ.

Influence of noise

Next, the multicomponent and pressure data are contaminated with Gaussian noise to evaluate the robustness of FWI with the different time-lapse strategies. The double-difference method is essentially designed to invert the data difference [eqs. (4) and (5)], for which the relative magnitude of the noise is much higher than for each data set separately. Hence, the time-lapse models produced by the double-difference method are distorted much more significantly compared to the two other techniques, and the actual time-lapse variations can be hardly identified from the inversion results (Figs. 6 and 7). Predictably, the resolution of the time-lapse variations reconstructed by all three methods decreases with the reduction in the signal-to-noise ratio (SNR; see Figs. 3, 6 and 7). With increasing level of noise, the amplitude of the time-lapse variations inside the "reservoir" for the parameters V_{P0}, ρ, and, especially, V_{S0} generally decrease (i.e., the changes in these parameters are underestimated). At the same time, the false anomalies in these parameters as well as in the velocities $V_{hor,P}$ and $V_{nmo,P}$ outside the target area become more pronounced (Figs. 6 and 7).

The time-lapse changes inside the target zone reconstructed by the parallel-difference method are more accurate than those obtained by the sequential-difference method. In contrast, the latter method performs slightly better outside the "reservoir" (Fig. 6 and Fig. 7). As in the previous test, the time-lapse models produced by all three methods have a lower resolution for the noisy pressure records than for the noisy multicomponent data.

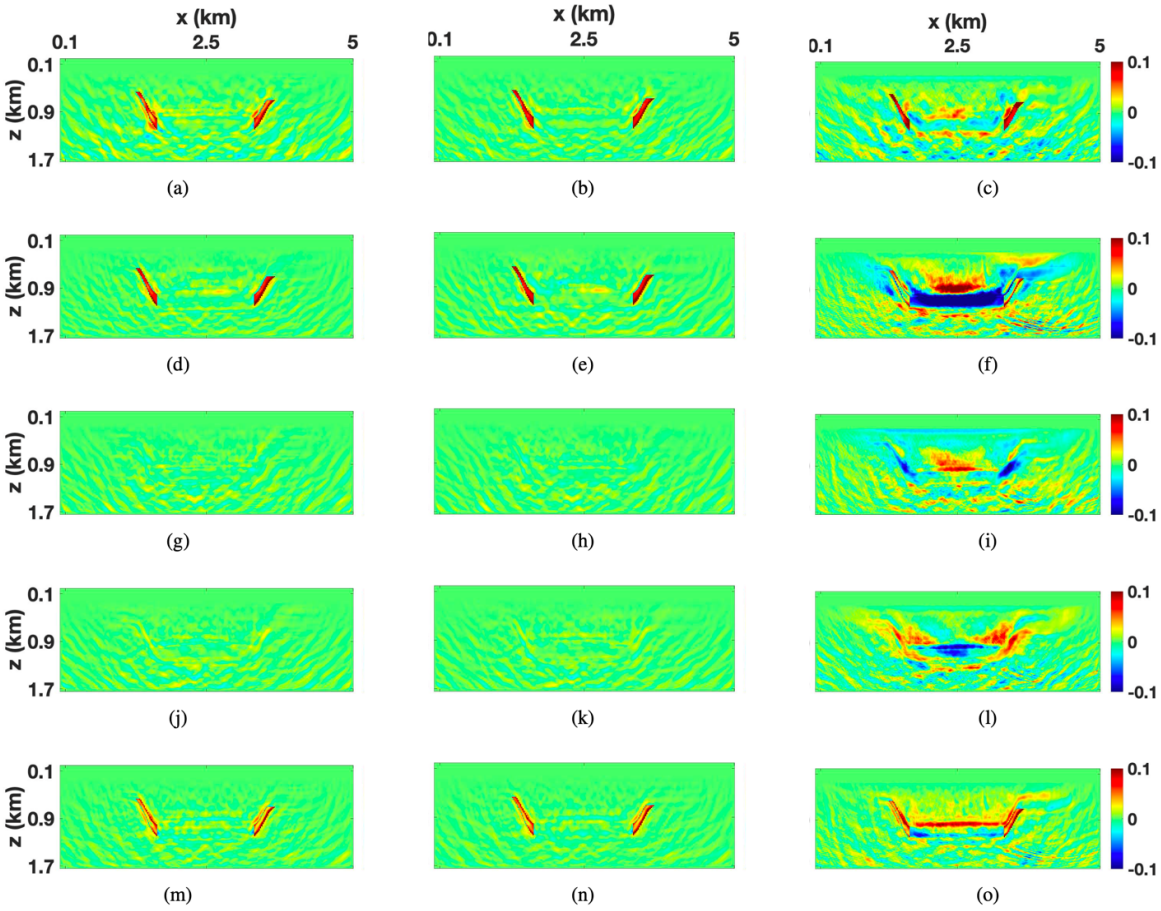

Fig. 6. Normalized errors of the time-lapse parameter variations obtained from the multicomponent data contaminated by Gaussian noise (the signal-to-noise ratio is 16). Only the parameters V_{P0}, V_{S0} and ρ are changed. The parallel-difference method: (a) V_{P0}, (d) V_{S0}, (g) $V_{hor,P}$, (j) $V_{nmo,P}$, and (m) ρ. The sequential-difference method: (b) V_{P0}, (e) V_{S0}, (h) $V_{hor,P}$, (k) $V_{nmo,P}$, and (n) ρ. The double-difference method: (c) V_{P0}, (f) V_{S0}, (i) $V_{hor,P}$, (l) $V_{nmo,P}$, and (o) ρ.

CONCLUSIONS

We extended elastic time-lapse FWI to VTI models which are typical, for example, for unconventional shale reservoirs. To resolve the temporal parameter variations, we employed three different time-lapse strategies previously proposed for isotropic media. Application of these methods to a

VTI graben model showed that none of them significantly outperforms the other techniques in reconstructing the time-lapse variations of the parameters $V_{P0,}$ $V_{S0,}$ and ρ (the P-wave NMO and horizontal velocities were held constant). For noise-free multicomponent data, the double-difference method produces the fewest artifacts outside the target zone because it focuses specifically on the time-lapse response. Still, a pronounced false anomaly in $V_{nmo,P}$ in the output of that method shows its susceptibility to parameter trade-offs (in this case, between the velocities V_{S0} and $V_{nmo,P}$).

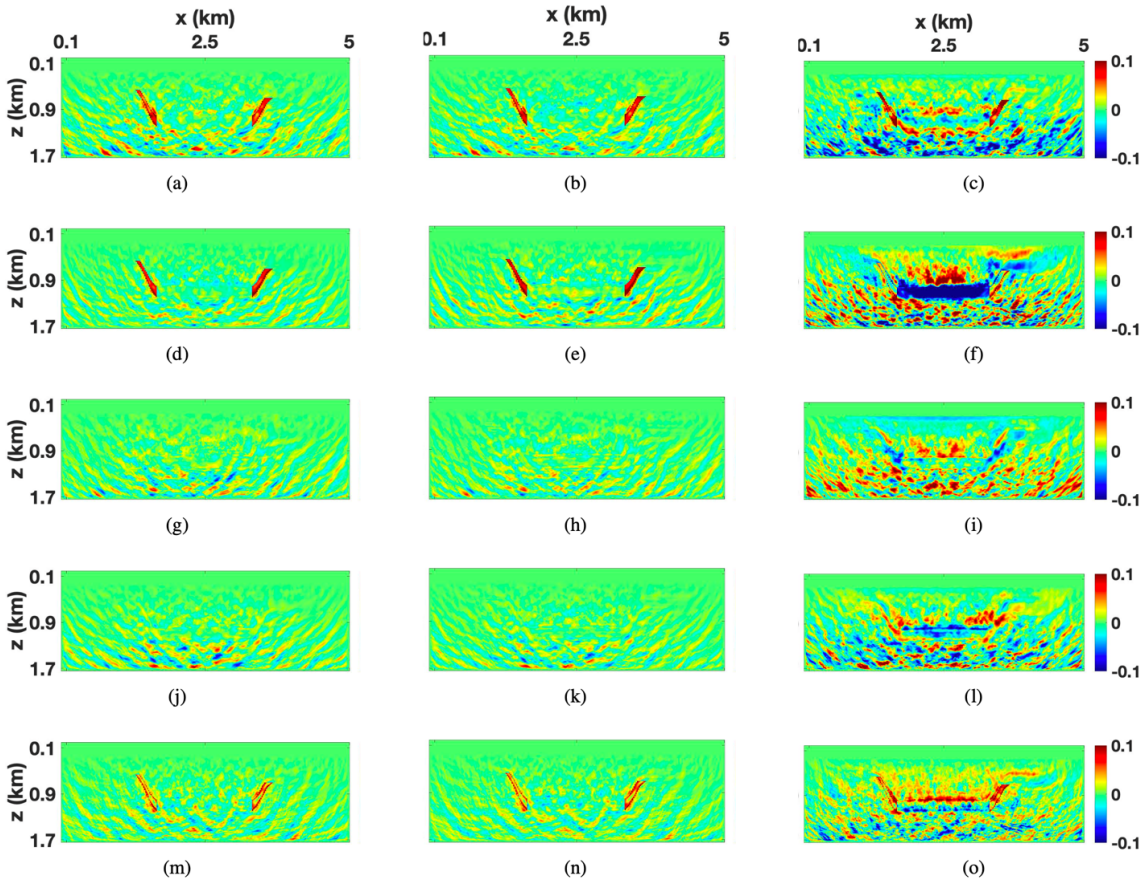

Fig. 7. Normalized errors of the time-lapse parameter variations obtained from the multicomponent data contaminated by Gaussian noise (the signal-to-noise ratio is 8). Only the parameters V_{P0}, V_{S0} and ρ are changed. The parallel-difference method: (a) V_{P0}, (d) V_{S0}, (g) $V_{hor,P}$, (j) $V_{nmo,P}$, and (m) ρ. The sequential-difference method: (b) V_{P0}, (e) V_{S0}, (h) $V_{hor,P}$, (k) $V_{nmo,P}$, and (n) ρ. The double-difference method: (c) V_{P0}, (f) V_{S0}, (i) $V_{hor,P}$, (*l*) $V_{nmo,P}$, and (o) ρ.

When FWI operates with noise-free pressure data, the parallel-difference method yields the most accurate results for $V_{P0,}$ $V_{S0,}$ and ρ due to the similarity between the errors for the baseline and monitor models. The parallel-difference and double-difference techniques generate comparable artifacts in the time-lapse variations of $V_{hor,P}$ and $V_{nmo,P}$ (which are

unchanged) caused by parameter trade-offs. The sequential-difference method, which is more sensitive to the errors in the inverted baseline parameters, does not perform well for the pressure data, which produce a low-resolution baseline model.

It is interesting that the false time-lapse anomaly in $V_{nmo,P,}$ which has a large magnitude for the multicomponent data, is much less pronounced when using the pressure records. Although multicomponent data help increase parameter resolution compared with the pressure inversion, they apparently make the objective function more multimodal, which hinders the convergence toward its global minimum.

When the data are contaminated by realistic Gaussian noise, the double-difference method fails to reconstruct the time-lapse variations because of the low signal-to-noise ratio of the difference between the monitor and baseline data. The parallel-difference method generally performs better than the sequential-difference method in reconstructing the time-lapse variations inside the target area but produces more artifacts outside the “reservoir”.

ACKNOWLEDGMENTS

We thank the members of the A(Anisotropy)-Team at the Center for Wave Phenomena (CWP) at Colorado School of Mines for useful discussions. We are grateful to Sagar Singh (CWP) for his kind help and suggestions. This work is supported by the Consortium Project on Seismic Inverse Methods for Complex Structures at CWP.

REFERENCES

Alemie, W. and Sacchi, M., 2016. Joint reparametrized time-lapse full-waveform inversion. Expanded Abstr., 86th Ann. Internat. SEG Mtg., Dallas: 1309-1314.

Asnaashari, A., Brossier, R., Garambois, S., Audebert, F., Thore, P. and Virieux, J., 2012. Time-lapse imaging using regularized FWI: a robustness study. Expanded Abstr., 82nd Ann. Internat. SEG Mtg., Las Vegas: 1-5.

Asnaashari, A., Brossier, R., Garambois, S., Audebert, F., Thore, P. and Virieux, J., 2015. Time-lapse seismic imaging using regularized full-waveform inversion with a prior model: Which strategy? Geophys. Prosp., 63: 78-98.

Bunks, C., Saleck, F.M., Zaleski, S. and Chavent, G., 1995. Multiscale seismic waveform inversion. Geophysics, 60: 1457-1473.

Denli, H. and Huang, L., 2009. Double-difference elastic waveform tomography in the time domain. Expanded Abstr., 79th Ann. Internat. SEG Mtg., Houston: 2302-2306.

Kamath, N. and Tsvankin, I., 2013. Full-waveform inversion of multicomponent data for horizontally layered VTI media. Geophysics, 78(5): WC113-WC121.

Kamath, N. and Tsvankin, I., 2016. Elastic full-waveform inversion for VTI media: Methodology and sensitivity analysis. Geophysics, 81(2): C53-C68.

Kamath, N., Tsvankin, I. and Díaz, E., 2017. Elastic full-waveform inversion for VTI media: A synthetic parameterization study. Geophysics, 82(5): C163-C174.

Lumley, D., 2010. 4D seismic monitoring of CO_2 sequenstration. The Leading Edge, 29: 150-155.

Maharramov, M. and Biondi, B., 2014. Joint full-waveform inversion of time-lapse seismic data sets. Expanded Abstr., 84th Ann. Internat. SEG Mtg., Denver: 954-959.

Pevzner, R., Urosevic, M., Popik, D., Shulakova, V., Tertyshnikov, E., Caspari, E., Correa, J., Dance, T., Kepic, A., Glubokovskikh, S., Ziramov, S., Gurevich, B., Singh, R., Raab, M., Watson, M., Daley, T., Robertson, M. and Freifeld, B., 2017. 4D surface seismic tracks small supercritical CO2 injection into the subsurface, CO2CRC Otway Project. Internat. J. Greenhouse Gas Contr., 63:150-157.

Plessix, R.-E., Michelet, S., Rynja, H., Kuehl, H., Perkins, C., Maag, J. and Hatchell, P., 2010. Some 3D applications of full waveform inversion. Expanded Abstr., 72nd EAGE Conf., Barcelona.

Singh, S., Tsvankin, I. and Zahibi Naeini, E., 2018. Bayesian framework for elastic full-waveform inversion with facies information. The Leading Edge, 37: 924-931.

Singh, S., Tsvankin, I. and Zahibi Naeini, E., 2019. Bayesian approach to facies-constrained waveform inversion for VTI media. Expanded Abstr., 89th Ann. Internat. SEG Mtg., San Antonio: 1370-1374.

Smith, S.S. and Tsvankin, I., 2013. Sensitivity of compaction-induced multicomponent seismic time shifts to variations in reservoir properties. Geophysics, 78(5): T151-T163.

Smith, S.S. and Tsvankin, I., 2016. Inversion of multicomponent seismic time shifts for reservoir pressure and length: A feasibility study. Geophys. Prosp., 64: 83-101.

Tarantola, A., 1984, Linearized inversion of seismic refection data. Geophys. Prosp., 32: 998-1015.

Thomsen, L., 1986. Weak elastic anisotropy. Geophysics, 51: 1954-1966.

Tsvankin, I., 2012. Seismic Signatures and Analysis of Refection Data in Anisotropic Media, 3rd ed. SEG, Tulsa, OK.

Vigh, D., Jiao, K., Watts, D. and Sun, D., 2014. Elastic full-waveform inversion application using multicomponent measurements of seismic data collection. Geophysics, 79(2): R63- R77.

Watanabe, T., Shimizu, S., Asakawa, E. and Matsuoka, T., 2004. Differential waveform tomography for time-lapse crosswell seismic data with application to gas hydrate production monitoring. Expanded Abstr., 74th Ann. Internat. SEG Mtg., Denver: 2323-2326.